DOI 10.1002/adhm.202301687

LIPID NANOPARTICLE DELIVERY ALTERS THE ADJUVANTICITY OF THE TLR9 AGONIST CpG BY INNATE IMMUNE ACTIVATION IN LYMPHOID TISSUE

Zifu Zhong,[a] Yong Chen,[a] Kim Deswarte,[b] Heleen Lauwers,[a] Emily De Lombaerde,[a] Xiaole Cui,[c] Simon Van Herck,[a] Tingting Ye,[a] Mark Gontsarik,[a] Stefan Lienenklaus,[d] Niek N. Sanders,[c] Bart N. Lambrecht,[b] Stefaan De Koker,[e] Bruno G. De Geest[a]*

[a] Dr. Zifu Zhong, Dr. Yong Chen, Heleen Lauwers, Emily De Lombaerde, Dr. Simon Van Herck, Tingting Ye, Dr. Mark Gontsarik, Prof. Bruno De Geest: Department of Pharmaceutics .Ghent University, Belgium. E-mail: br.degeest@ugent.be

[b] Kim Deswarte, Prof. Bart N. Lambrecht. Department: Department of Internal Medicine and Pediatrics. Ghent University, VIB Center for Inflammation Research, Ghent, Belgium

[c] Xiaole Cui, Prof. Niek N. Sanders. Laboratory of Gene Therapy Ghent University, Belgium.

[d] Dr. Stefan Lienenklaus . Institute for Laboratory Animal Science and Institute of Immunology. Hannover Medical School

[e] Dr. Stefaan De Koker . eTheRNA Immunotherapies

ABSTRACT

Pharmacological strategies to activate innate immune cells are of great relevance in the context of vaccine design and anti-cancer immune therapy, to mount broad immune responses able to clear infection and malignant cells. Synthetic CpG oligodeoxynucleotides (CpG-ODNs) are short single-stranded DNA molecules containing unmethylated CpG dinucleotides and a phosphorothioate backbone. Class B CpG ODNs activate robust innate immune responses through a TLR9-dependent NF-κB signaling pathway. This feature is attractive to exploit in the context of vaccine design and cancer immunotherapy. Soluble CpG-ODNs cause hepatic toxicity, which reduces its therapeutic applicability. We report on the formulation of class B CpG ODN1826 in lipid nanoparticles (LNPs) containing an ionizable cationic lipid that complexes CpG through electrostatic interaction. Upon local administration, LNP-formulated CpG drains to lymph nodes and triggers robust innate immune activation. Unformulated, soluble, CpG, by contrast, is unable to induce robust innate activation in draining lymph nodes and is distributed systemically. In a vaccination setting, LNP-formulated CpG, admixed with a protein antigen, induces higher antigen-specific antibody titers and T cell responses than antigen admixed with unformulated soluble CpG.

INTRODUCTION

Vaccination is ubiquitous in preventing and controlling the spread of infectious agents and is also emerging as an anti-cancer immunotherapy. Most synthetic peptide or recombinant protein subunit antigens derived from proteins of the viral capsid or neo-antigens that result from somatic mutations in cancer cells are poorly immunogenic. Consequently, these proteins and peptides are unable to induce robust humoral and cellular antigen-specific immune responses to protect the host. Successful vaccine design requires co-formulation of antigen with adjuvants that activate the innate immune system.[1] Bacterial and viral nucleic acids, and their synthetic analogues are recognized by innate immune cells through a large family of germline-encoded pattern-recognition receptors (PRRs) including Toll like receptors (TLRs).[2] Triggering of PRRs activates various innate signaling pathways leading to the production of type I interferons (IFN), proinflammatory cytokines, and antimicrobial peptides.[2b, 3] In presence of an external or endogenous antigen, TLR triggering can skew and amplify the magnitude of the antigen-specific adaptive immune response. TLR agonists are currently being explored as an adjuvant in vaccine design, but also as a drug for the treatment of infectious diseases and for cancer immunotherapy.

Synthetic short single-stranded oligodeoxynucleotides (ODNs) containing unmethylated cytosine-guanine (CpG) motifs are potent agonists of TLR9. TLR9 is expressed in various immune cell subsets, including dendric cells (DCs) and B cells.[4] Triggering of TLR9 induces a signaling cascade by activating the myeloid differentiation primary-response protein 88 (MyD88) and downstream nuclear factor kappa-B (NF-κB) pathways. CpG ODNs induce robust T helper-1 (Th1)-type immune responses characterized by the secretion of pro-inflammatory cytokines such as IFN-γ, interleukin (IL)-6 and IL-12.[5] Co-administration of antigen with CpG ODNs increases antigen-specific antibody titers and cytotoxic T cells levels.[1d, 6]

CpG ODNs have been evaluated in multiple (pre)clinical studies.[6a, 7] CpG 7909, (PF-3512676; ProMune®) has been evaluated in phase III trial in combination with chemotherapy for treatment of non-small-cell lung cancer.[8] Recently, CpG 1018 was approved by the FDA as the first licensed CpG-based adjuvant for human vaccine use in the Hepatitis B Vaccine, HEPLISAV-B®.[9] Although proven to be effective and safe in clinical trials, CpG ODNs are administered in unformulated, soluble, form. This is suboptimal due to rapid diffusion from the injection site into systemic circulation. Consequently, uncontrolled off target innate immune activation and apoptosis in hepatocytes is caused,[1d, 10] which strongly reduces the therapeutic window of CpG ODNs. Indeed, subcutaneous administration of a soluble formulation of CpG ODN, i.e. PF-3512676, failed to improve the treatment efficacy in patients in a phase III clinical trial.[8] Hence, a need exists to develop more safe and more

therapeutically efficient strategies to deliver CpG ODNs. Formulation of CpG ODNs into nanoparticles can improve its adjuvanticity, by focusing its' activity on the relevant antigen presenting cells in draining lymphoid tissue.[10-11]

Class B CpG ODNs, such as CpG ODN1826, have a phosphorothioate backbone which improves resistance to nucleases, and thereby prolongs half-life in vivo. CpG ODN1826 activates DCs and thereby promotes CD8+ T cell immunity, but also stimulates the phagocytic activity of macrophages and activates B cells to increase antibody responses and antibody isotype switching.[4b, 6a, 7],[12] Here, we formulated CpG ODN1826 into lipid nanoparticles (LNP) containing an ionizable cationic lipid that binds the CpG though electrostatic interaction and hydrogen bonding.[13] LNPs are considered as the state-of-the-art delivery technology for macromolecular nucleic acid drugs. LNPs have reached the clinic for the siRNA drug product Onpattro® and the Moderna and BioNTech mRNA COVID-19 vaccine products. Notably, by themselves, i.e. without any nucleic acid drug payload, LNP also were reported to possess fairly potent vaccine adjuvant properties.[14]

In this paper, we made use of S-Ac7-DOG as an ionizable lipid. S-Ac7-DOG was identified in our laboratories during a recent screening of a combinatorial library of ionizable lipids for mRNA delivery,[15] and contains a self-immolative disulfide bond that can be cleaved in response to intracellular reductive triggers. In vitro, we investigated cellular interaction and TLR agnostic activity. In vivo, in mice, we demonstrated that local administration of CpG in LNP targets antigen presenting cells in draining lymph nodes and reduces systemic dissemination of CpG with a concomitant reduction in systemic innate activation. In an immunization setting we demonstrated that adjuvating a model protein antigen with CpG in LNP augmented the amplitude the antibody responses and induces isotype switching towards higher IgG2 titers. Adjuvanting antigen with CpG in LNP also increased the generation of antigen-specific CD8+ T cell responses.

RESULTS AND DISCUSSION

CpG ODN can be formulated in LNP using standard LNP formulation conditions

The class B CpG ODN1826, further denoted as CpG, was encapsulated in LNP by rapid mixing under vigorous stirring of an acetate buffer (5 mM, pH 4.5) containing CpG with an ethanolic solution containing the ionizable lipid S-Ac7-DOG, cholesterol, phospholipid (DOPE or DSPC) and poly(ethylene glycol)-lipid (DMG-PEG or DSG-PEG; in both cases PEG had an MW of 2 kDa) at a 50:38.5:10:1.5 ratio (Figure 1). DSPC and DOPE are both zwitterionic phospholipids. DSPC comprises saturated acyl chains and a larger N-methylated head group while DOPE comprises two unsaturated alkyl tails and a smaller primary amine head group. DMG-PEG and DSG-PEG share a similar structure but different length of the unsaturated alkyl tail, comprising

14 and 18 carbons, respectively. DSG-PEG has been reported to remain more firmly associated to the LNP surface in a complex physiological medium, whereas DMG-PEG was reported to be released from the LNP surface and become replaced by serum proteins.[16] This feature was reported to alter the pharmacokinetic profile of LNP.[16] After mixing, LNP were dialyzed against PBS to remove the ethanol and increase the pH of the medium to 7.4. In total 8 different CpG LNP formulations and a control LNP formulation without CpG were produced, targeting an N/P (ionizable Nitrogen atoms of the ionizable lipid to anionic Phosphor atoms of CpG) molar ratio of respectively 10:1 and 5:1. The parameters of the respective LNP formulations are listed in Table 1.

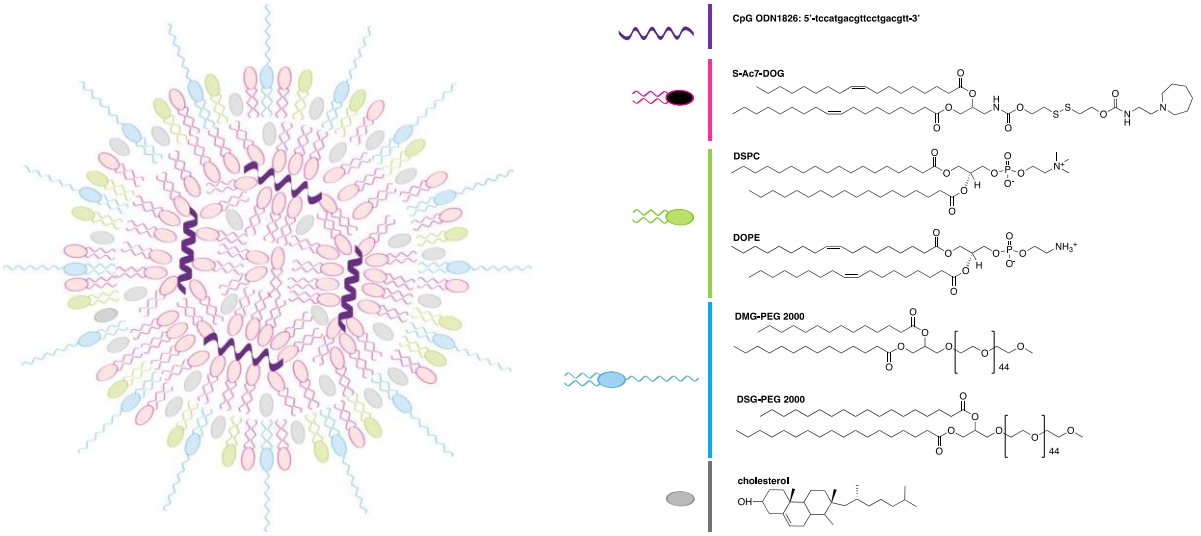

Figure 1. LNP composition. Schematic representation of CpG LNP, the nucleotide sequence of CpG ODN1826 and molecular structure of the LNP components: ionizable lipid S-Ac7-Dog, DSPC, DOPE, DMG-PEG-2000, DSG-PEG 2000 and cholesterol.

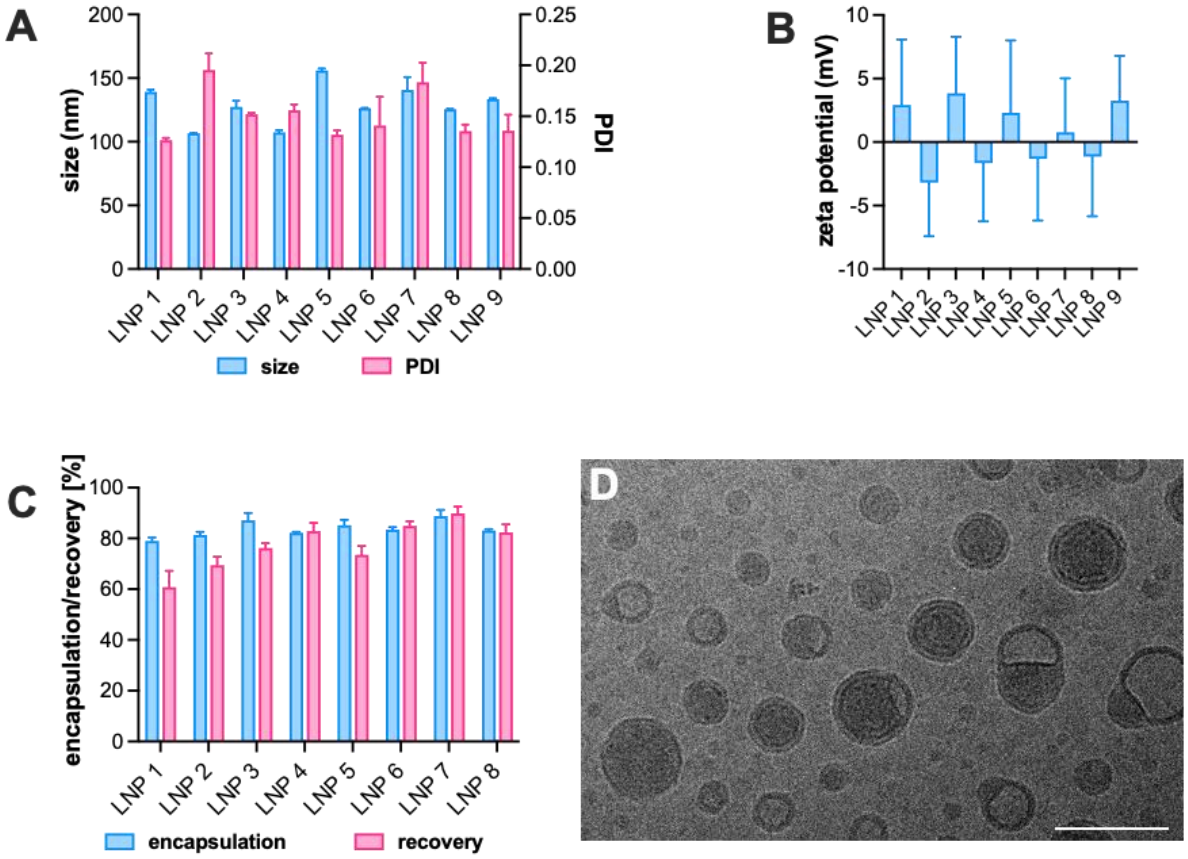

Figure 2. LNP characterization. (A) DLS analysis of Z-average diameter and PDI, (B) zeta-potential and (C) encapsulation efficiency and recovery of LNP formulations measured by OliGreen assay (n=3, mean ± SD). Statistical analysis is shown in Table S1 in the Supporting Information section. (D) Cryo transmission electron microscopy image of CpG-LNP (LNP7: DSPC/DSG-PEG/10:1). Scale bar represents 90 nm.

Table 1. Overview of LNP formulation parameters.

	ethanolic phase						aqueous phase	N/P ratio	
LNP	S-Ac7-DOG	Cholesterol	DMG-PEG	DSG-PEG	DOPE	DSPC	CpG ODN1826	10	5
Soluble CpG	-[a]	-	-	-	-	-	+[b]	-	-
LNP1	+	+	+	-	+	-	+	+	-
LNP2	+	+	+	-	+	-	+	-	+
LNP3	+	+	-	+	+	-	+	+	-
LNP4	+	+	-	+	+	-	+	-	+
LNP5	+	+	+	-	-	+	+	+	-
LNP6	+	+	+	-	-	+	+	-	+
LNP7	+	+	-	+	-	+	+	+	-
LNP8	+	+	-	+	-	+	+	-	+
LNP9	+	+	+	-	-	+	-	+	-

Note: [a]: presence; [b] : absence

Dynamic light scattering (DLS) analysis of CpG-LNP indicated a diameter ranging from 100-150 nm and a low polydispersity index (PDI) (i.e. <0.2) (Figure 2A). Of note, LNPs within this size range were reported to exhibit excellent cell uptake, immunogenicity and safety in vivo.[17] The zeta-potential values of the LNPs, measured at neutral pH, ranged between -10 and +10 mV (Figure 2B). LNPs with an N/P ratio of 5 were slightly negatively charged. LNPs with an N/P ratio of 10 were slightly positively charged. CpG encapsulation efficiency was determined using the Quanti-it OliGreen assay, indicating an encapsulation efficiency of CpG in LNP between 80 and 90%. The recovery rate (i.e. the amount of CpG measured in the formulation after disassembly of the LNP by addition of Triton-X, relative to the theoretical total amount of CpG in the formulation) varied between 70 and 85% (Figure 2C). Cryo transmission electron microscopy revealed that CpG-LNPs exhibit polydisperse nanoscopic morphological features comprising both single bilayer and all bilayer structures (Figure 2D; exemplified for LNP7). Notably, differences in morphology between individual LNP, including bleb formation has

recently been attributed to occur during buffer exchange.[18] Interestingly, in the context of mRNA delivery, such bleb formation has been a found to improve transfection efficiency.

LNP formulation has a moderate effect on the TLR agonistic activity of CpG ODN in vitro

The effect of LNP formulation on the TLR9 agonistic activity of CpG was assessed using the Raw-Blue NF-κB reporter cell assay. The latter is derived from RAW 264.7 macrophages containing a secreted embryonic alkaline phosphatase (SEAP) reporter gene that can be induced by NF-κB. Uptake of CpG by Raw-Blue cells followed by triggering of TLR9 in endosomal vesicles activates a signaling cascade, resulting in the secretion of SEAP into the cell medium. SEAP concentration can be measured using a colorimetric assay. CpG-LNP formulated with DMG-PEG exhibited (Figure 3A-B) a higher potency compared to unformulated soluble CpG. CpG-LNP formulated with DSG-PEG were equally potent as unformulated soluble CpG. Empty LNP that did not contain CpG did not induce a detectable response, indicating that this class of LNP does not induce NF-κB activation in RAW cells within the tested experimental window. LNP with an N/P ratio of 10/1 ratio had a lower EC50 compared to LNP with an N/P ratio of 5/1, which might be caused by enhanced cellular uptake due to their positive surface charge. Regarding the role of the phospholipid in the LNP formulation, no significant difference was observed between CpG-LNP formulated with DOPE or DSPC, respectively. Cytotoxicity of the CpG-LNP formulations was assessed in DC2.4 cells, an immortalized mouse dendritic cell line, using the MTT assay. Relative to soluble CpG, CpG-LNP showed increased cytotoxicity at the highest tested CpG concentration of 3 µg/mL (corresponding to an ionizable lipid concentration of 100 µg/mL). We attribute this toxicity to the LNP itself as empty LNP provoked a similar cytotoxicity profile (Figure 3C). Notably, empty LNP did not exhibit TLR agonistic activity within the tested concentration range (Figure S1).

At this stage, a selection of CpG-LNP formulations was made for further evaluation. We decided continuing with CpG-LNP containing DSPC as phospholipid based on the lack of benefit of using DOPE and the fact that DSPC is present in the clinically approved OnPattro siRNA drug product and in both the BioNTech/Pfizer and Moderna mRNA vaccines.[13a, 19] We also decided continuing with CpG-LNP comprising an N/P ratio of 10 based on their higher in vitro potency. For further evaluation we included both DMG-PEG and DSG-PEG.

LNP formulation moderately affects CpG ODN behaviour in vitro

Cellular association of CpG-LNP was measured by flow cytometry using FITC-labeled CpG (further denoted as FITCCpG). DC2.4, an immortalized mouse dendritic cell line, was used as a model for antigen presenting cells. Flow cytometry showed cellular association of FITCCpG-LNP and unformulated soluble FITCCpG after overnight incubation (Figure 4A). Cells treated with DMG-PEG FITCCpG-LNP exhibited a slightly higher cellular fluorescence compared to

cells treated with unformulated, soluble, FITCCpG and DSG-PEG FITCCpG-LNP. LNP exhibited positive zeta potential values at neutral pH (Figure 4A), which can be attributed to a pKa value of 6.8, measured by 2-(p-toluidino) naphthalene-6-sulfonic acid (TNS) assay (Figure S2). LNP containing DMG-PEG were reported to readily exchange their PEG-coating with serum proteins, in serum-rich conditions, whereas DSG-PEG remains firmly bound to the LNP surface.[20] Hence, it is likely that adsorption of serum proteins to the slightly positively charged DMG-PEG CpG-LNP increased cellular uptake.

Regarding the comparison between FITCCpG and FITCCpG-LNP, we want to note that it is difficult to draw quantitative conclusions from the flow cytometry data due to counteracting phenomena occurring during LNP formulation and cellular uptake. Indeed, FITC fluorescence is partially quenched inside LNP due to confinement of the FITCCpG molecules within a small volume. Upon endocytosis in endosomes, the local acidic pH can further reduce FITC fluorescence. LNP disassembly can release FITCCpG in a soluble form, which would lead to fluorescence dequenching. Hence, we deliberately opt to not over-interpret the flow cytometry data.

Confocal microscopy (Figure 4B) confirmed that both FITCCpG and FITCCpG LNP were effectively internalized by cells. The observed punctuated pattern is characteristic for endosomal localization. From flow cytometry and microscopy experiments it can be concluded that LNP formulation did not dramatically alters cellular uptake in vitro, at least not within the chosen experimental window.

CpG-LNP induces local type I interferon activation in draining lymph nodes in vivo

CpG ODN1826 induces type I IFN and IL-6 production in vivo, which are key cytokines in shaping innate and adaptive immunity.[21] We used an IFN-β+/Δβ-luc IFN-β luciferase reporter mouse model to screen the effect of LNP formulation on the magnitude and biodistribution of the CpG-induced type I IFN response. This transgenic mouse model carries a firefly luciferase reporter gene linked to IFN-β.

An equivalent dose of 2 µg CpG in unformulated soluble or LNP-formulated form was injected subcutaneously (SC) into the footpad of IFN-β+/Δβ-luc mice and bioluminescence imaging was performed 4, 24 and 48 h post injection. The SC route of administration was chosen due the popliteal lymph node being the single draining lymph node, hence facilitating discrimination between systemic and more localized innate immune activation (Figure 5A). Unformulated soluble CpG induced at 4 h postinjection only a bioluminescence signal at the site of injection in the footpad. At 24 and 48 h post injection, the signal in the footpad was increased. Also, a distal signal emerged in the liver at 24 h. Empty LNP, induced a weak signal in the footpad which did not change over time and did not differ between DMG-PEG and DSG-PEG LNP.

CpG LNP induced an IFN-β response in the draining popliteal lymph node and an increased signal in the liver and spleen after 24 h. After 48 h the signal decreased again, indicating a transient nature of the innate immune activation (Figure 5). CpG-LNP containing DSG-PEG were more potent in inducing IFN-β than CpG-LNP containing DMG-PEG. The ratio of the local to the total bioluminescence of the IFN-β related luciferase signal identified CpG-LNP containing DSG-PEG to be the most potent type I interferon inducing formulation in vivo. Therefore, the CpG-LNP formulation containing DSG-PEG was selected for further evaluation.

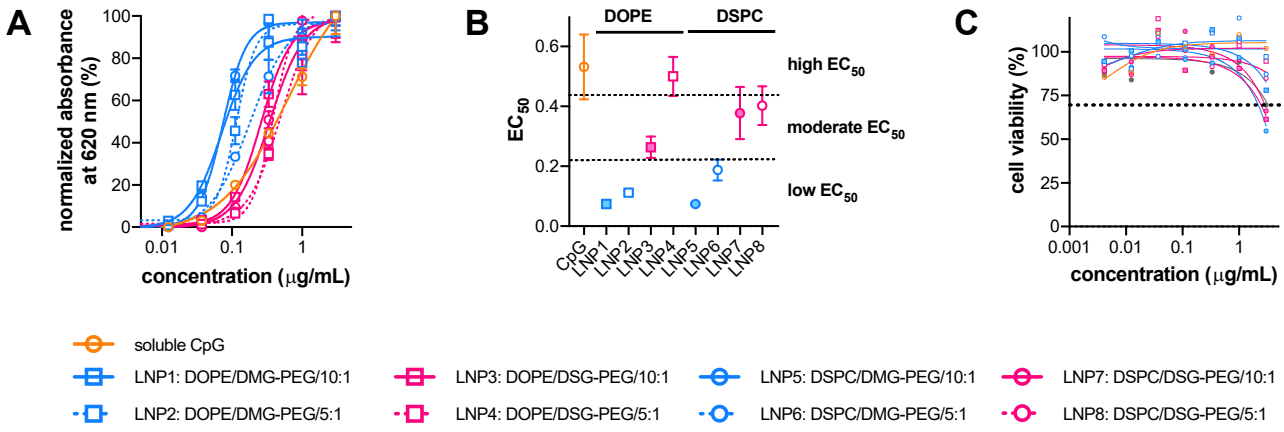

Figure 3. In vitro evaluation of TLR agonistic activity and cytotoxicity. (A) TLR agonistic activity of LNP formulations measured as NF-kB activation by a RAW-Blue reporter assay. (n=6, mean ± SD). (B) EC50 values of LNP formulation calculated from the dose response curves in panel (A). Statistical analysis is shown in Table S2 in the Supporting Information section. (C) Cytotoxicity of LNP on DC2.4 cells formulations measured by MTT assay (n=4).

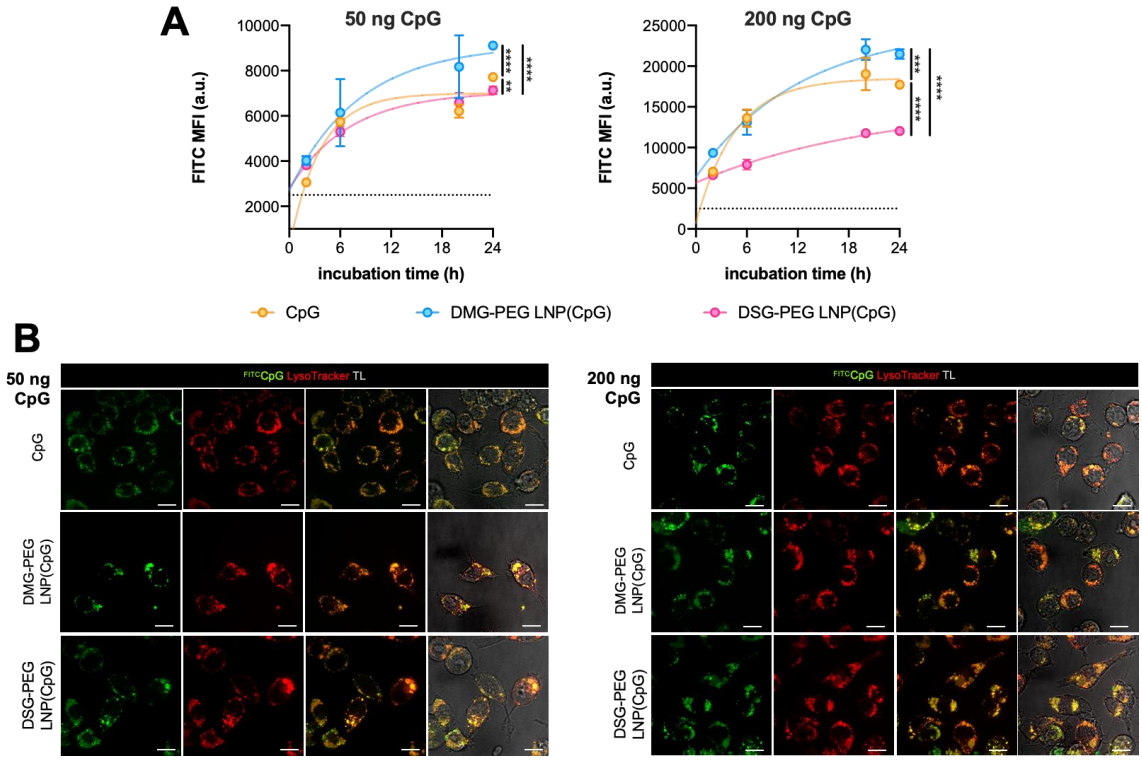

Figure 4. In vitro evaluation of cellular uptake. (A) Flow cytometry analysis of DC2.4 cells incubated with FITCCpG-LNP and unformulated soluble FITCCpG. The dashed line represents the MFI value of untreated cells. Statistical analysis by two-way ANOVA is shown for the last time point. For other time points, statistical analysis is shown in Table S3 in the Supporting Information section.; ****:p<0.0001, ***:p<0.001, **:p<0.01.(B) Corresponding confocal microscopy images comprising the green fluorescence channel (FITCCpG), and an overlay of the green and blue (Hoechst: cell nuclei) fluorescence channels and the transmitted-light channel. Scale bar: 15 microns.

We then tested the effect of LNP-formulation on the type I IFN response upon intramuscular injection (IM) of CpG-LNP in the gastrocnemius muscle, as this route of administration is relevant in a vaccination context. IM injection of unformulated CpG (10 µg dose) resulted in a robust type I IFN response in the liver, accounting for over 50% of the total bioluminescence (Figure 5D-F). These results are in line with previous report in literature on systemic dissemination of soluble CpG[22] and on strong innate immune activation in the liver, leading to T cells infiltration and hepatic toxicity.[23]

Interestingly, we observed that treatment of IFN-β reporter mice with free CpG admixed with empty LNP induced a qualitatively similar, albeit slightly quantitatively slightly lower response compared to CpG-LNP (Figure 5F1-F2). We attribute this phenomenon to the binding of CpG to the cationic surface of the LNP through electrostatic interactions (Figure S3). Admixing free CpG with empty LNP represents a straightforward method that yields a similar encapsulation efficiency and recovery rate of CpG as CpG-LNP. Notably, the addition of CpG to empty LNP

did not alter the physical size of the LNP nanoparticles, with the LNP size primarily influenced by the N/P ratio. In contrast, the physical size of CpG-LNP remained consistent across different N/P ratios (Figure S4). Further investigations and optimization efforts are required to effectively employ the admixing of CpG with empty LNP in future applications.

Note that for the IM route of administration, compared to the SC route, a 5-fold higher dose was administered due to the higher available volume for IM injection and 10 µg being the envisioned dose in a vaccination setting (vide infra). Importantly, intramuscular administration of CpG-LNP induced, compared to soluble CpG, much less innate activation in the liver and provoked a durable response at site of administration in the muscle (Figure 5). Considering the comparable performance of CpG-LNP and CpG admixed with empty LNP, we have chosen to prioritize CpG-LNP for further investigation. This approach is more standardized and, consequently, holds higher translational potential.

CpG-LNP targets DCs in lymph nodes and induces broad innate immune activation

To profile the innate immune response elicited by empty LNPs, soluble CpG and CpG-LNPs, we analyzed the vaccine draining lymph node (dLN) by flow cytometry. dLNs were isolated 24h after SC injection in the footpad or IM injection in the gastrocnemius. FITCCpG was used to determine which cells ingested CpG.

In line with previous reports, injection of soluble CpG led to activation of cDCs in the dLN, evidenced by an increased expression of CCR7 – the chemokine receptor promoting DC migration towards lymphoid tissue – and increased levels of the co-stimulatory molecules CD80 and CD86 (Figure 6A). Similar patterns were observed in the cDC1 and cDC2 populations. Soluble CpG also provoked CD69 upregulation on B cells, which are known to express TLR9. Empty LNPs in contrast had no significant impact on the activation status of cDCs, B cells and T cells in the dLN. LNP mediated delivery of CpG enhanced, compared to soluble CpG, immune activation in dLNs, with higher expression levels of CCR7, CD80 and CD86 on cDC populations, a marked increase in CD69 expression on T cells, and a moderate increase in CD69 on B cells. Overall, similar trends were observed for SC and IM injection. We conclude, based on the obtained IFN-β luciferase reporter bioluminescence and flow cytometry data that local injection of CpG-LNP induces, relative to unformulated, soluble, CpG, stronger activation of a broad range of immune cell subsets in the draining lymph node.

Analysis of the FITC signal (Figure 6B) revealed that a large proportion of the cDC1 and cDC2 populations had ingested CpG, with little differences observed between soluble and LNP formulated CpG. SC injection conferred higher percentages of FITC-CpG positive cDCs in the draining popliteal lymph node, compared to the percentage of FITCCpG positive cDCs in the draining iliac lymph node upon IM injection. This is likely due to distribution over multiple lymph

nodes and/or reduced mobility in muscle tissue compared to subcutaneous tissue. FITCCpG positive cDC1s typically expressed high levels of CD80 and CD86, but these markers were also increased on FITCCpG negative DCs (Figure 6C), suggesting DC maturation/activation can occur “in trans” via the release of immune-stimulatory cytokines such as type I IFN. Only minor percentages of B cells (0.5-1%) and T cells (0.2-0.5%) were positive for FITCCpG. Nonetheless, high levels of CD69+ T-and B-cells were seen in response to CpG-LNP treatment, pinpointing towards potent indirect effects of CpG on T-and B-cell activation, either mediated by cytokines or cell-cell interaction between lymphocytes and activated cDCs.

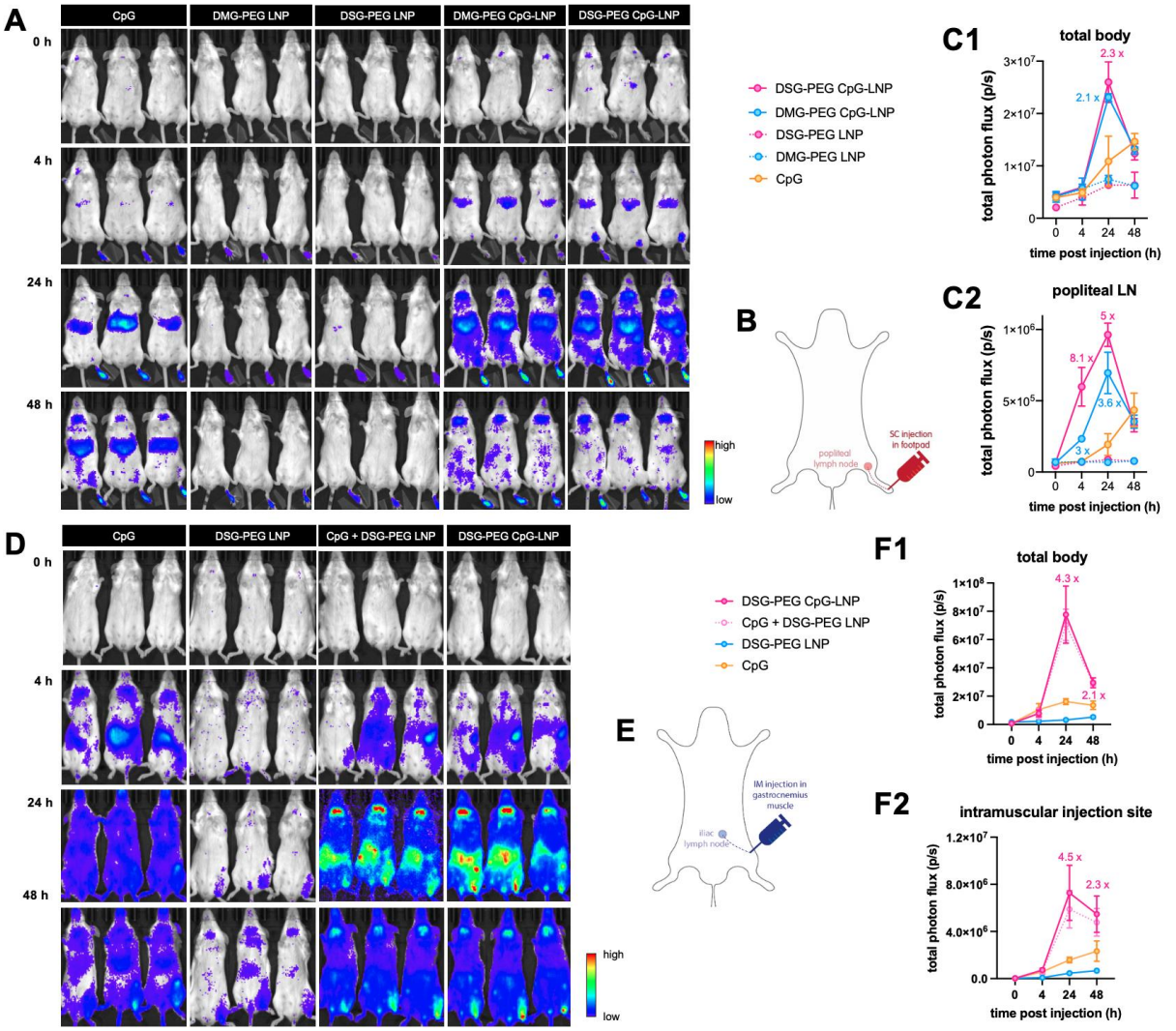

Figure 5. Tissue level analysis of the in vivo innate immune activation of CpG-LNP. LNP were formulated with DSPC, and DMG-PEG or DSG-PEG, respectively, at an N/P of 10. (A) Bioluminescence images of IFN-β luciferase reporter (IFN-β+/Δβ-luc) mice; images taken 0, 4, 24 and 48 h post footpad injection. (B) Schematic illustration of the subcutaneous injection site and draining popliteal lymph node. (C) Quantification of the bioluminescence signal post footpad injection (n=3, mean ± SD) ROI’s were assigned according to Figure S4 in the supporting Information section. (D) Bioluminescence images of IFN-β+/Δβ-luc mice; images taken 0, 4 and 24 h post intramuscular injection. (E) Schematic illustration

of the intramuscular injection site and draining iliac lymph node. (F) Quantification of the bioluminescence signal post intramuscular injection (n=3, mean ± SD). Fold increase between CpG-LNP and soluble CpG are annotated.

LNP formulation enhances adjuvanticity of CpG in a vaccination context

Cohorts of C57BL/6 mice received an intramuscular injection of 50 µg ovalbumin (OVA, used as a model antigen) admixed with an equivalent dose of 10 µg CpG in LNP and in unformulated, soluble form. Empty LNP and unadjuvanted OVA and PBS were included as controls. A prime and boost immunization scheme with an interval of three weeks (Figure 7A) was selected. Serum samples were collected 3- and 6-week post-immunization. OVA-specific total IgG antibody titers and IgG1/IgG2c antibody subclass titers were quantified by calculating the area under curve (AUC) values of the respective dilution series (Figure 7B). LNP-CpG adjuvanted antigen induced significantly higher anti-OVA IgG titers and IgG2c, but not IgG1, both after prime and boost immunization, compared to antigen adjuvanted with unformulated soluble CpG. This suggests that the LNP-CpG potently skews Th1 type immunity. Th1-dominant immunity is particularly beneficial for combating intracellular pathogens such as viruses, bacteria, and parasites. It also plays a role in inducing autoimmunity and anticancer cellular responses, improving vaccination efficacy, and promoting long-term immunity. Mice injected with non-adjuvanted antigen failed to develop detectable antigen-specific antibody titers. Interesting, adjuvating antigen with empty LNP also mounted elevated IgG1 subclass titers. This intrinsic adjuvant activity of LNP is in line with a recent report on the capacity of LNP, although containing another ionizable lipids than in our LNP formulations, to promote induction of robust T follicular helper cells.[14] Overall, booster immunization increased antibody titers without altering the qualitative differences between the respective immunization cohorts.

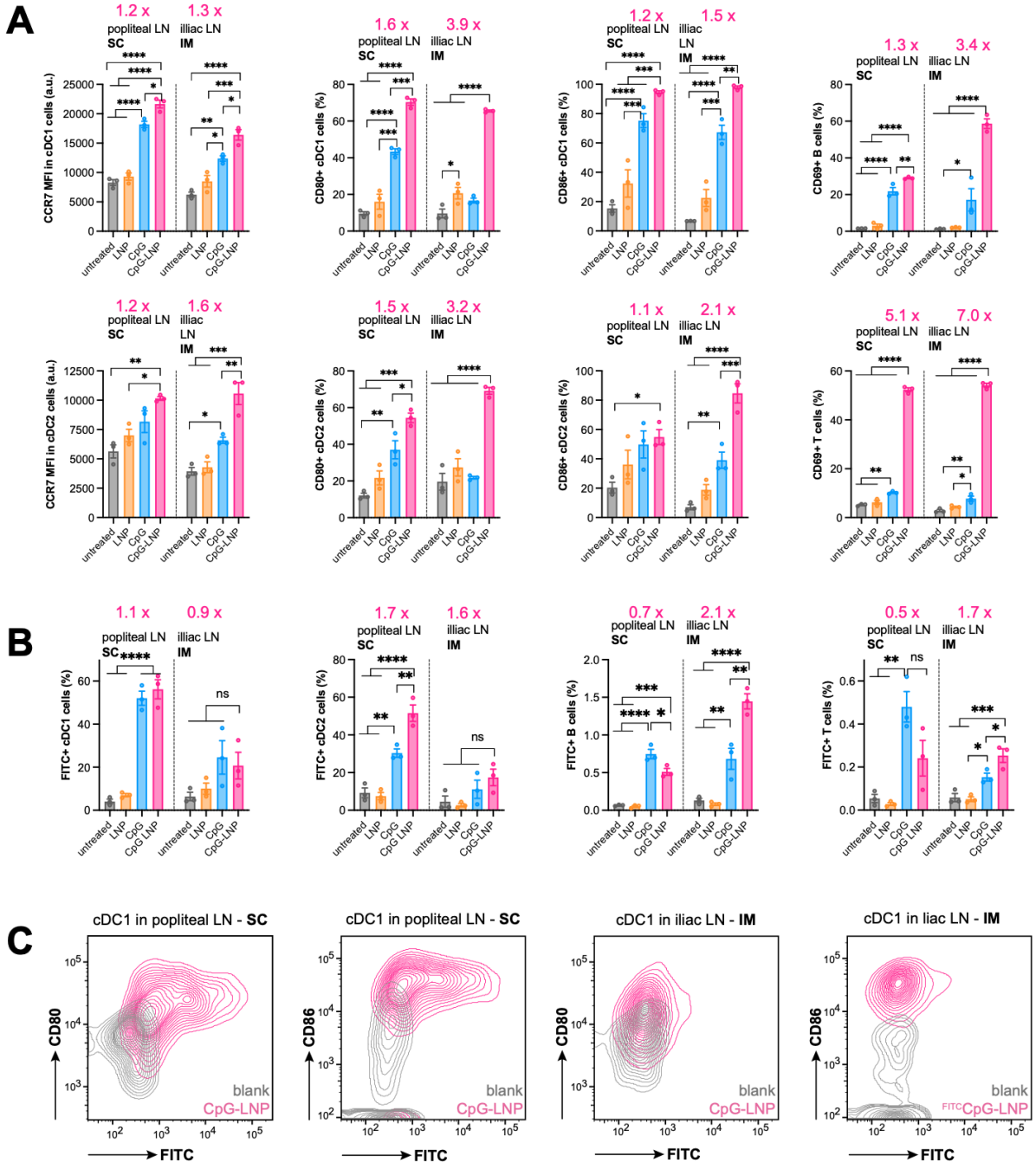

Figure 6. Cellular level analysis of the in vivo innate immune activation of CpG-LNP. LNP were formulated with DSPC, and DMG-PEG or DSG-PEG, respectively, at an N/P of 10. Flow cytometry analysis of (A) maturation and activation markers and (B) FITC association in immune cell subsets in the draining popliteal and iliac lymph nodes, 24 h post subcutaneous or intramuscular injection, respectively, of IFN-β+/Δβ-luc mice (n=3, mean ± SD). Statistical analysis by one-way ANOVA; ****:p<0.0001, ***:p<0.001,**:p<0.01;*:p<0.05. Fold increase between CpG-LNP and soluble CpG are annotated. (C) Flow cytometry density plots of the FITC signal versus the maturation markers CD80 and CD86, respectively, in the cDC1 DC subset, post subcutaneous and intramuscular injection of CpG-LNP. Untreated lymph nodes are depicted as control.

The presence of antigen-specific cytotoxic CD8+ T cells in the spleen was investigated one-week post immunization with a second booster. Flow cytometry analysis with tetramer staining on single cell suspensions prepared from the dissected spleens indicated (Figure 7C) that CpG-LNP adjuvanted antigen induced a two-fold increase in the percentage of antigen specific CD8+ T cells compared to antigen adjuvanted with unformulated soluble CpG and empty LNP.

Multiplex cytokine analysis of serum samples collected 6 h post the booster immunization (Figure 7D), revealed that immunization with CpG-LNP induced the highest levels of the cytokines IFN-γ, IL-6, IL-10 and IL-12, and the chemokine MCP-1. In this experimental setting, cytokine secretion was measured in response to the combined effect of TLR9 triggering and re-exposure of B and T cells to antigen. The synergy between these events might account for the markedly higher cytokines levels in the serum of CpG-LNP adjuvant mice. Notably, TNF-a, a cytokine associated with tissue damage, was detected in none of the groups (Figure S5).

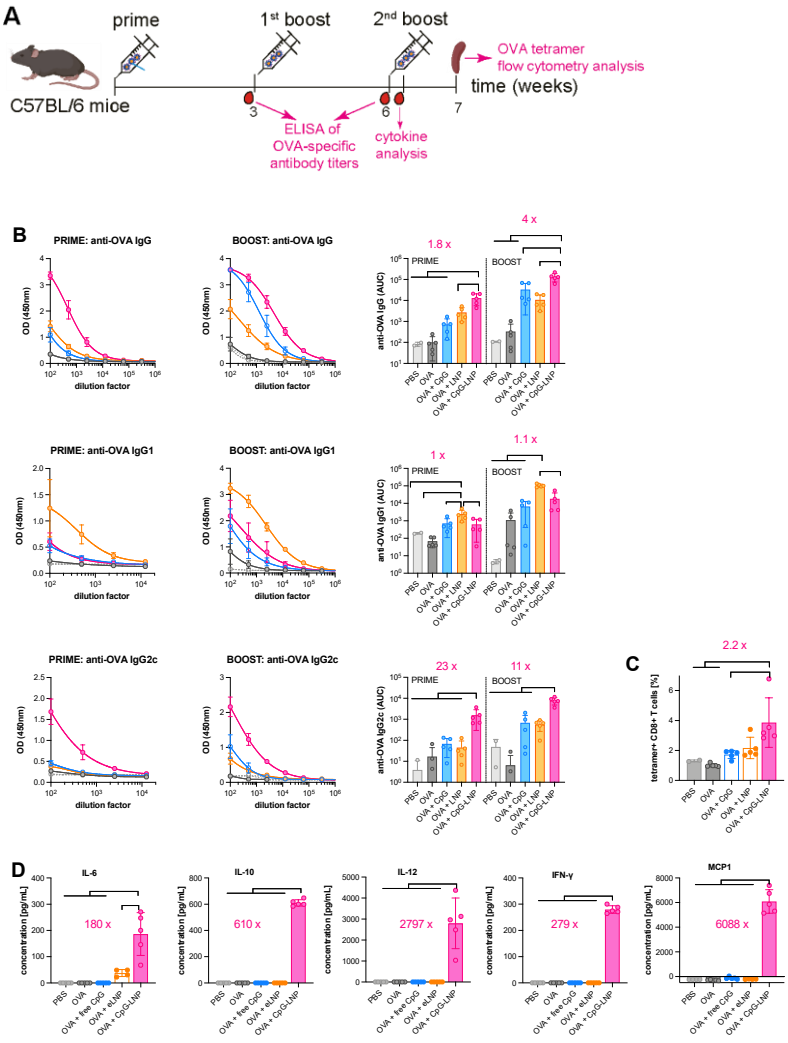

Figure 7. In vivo adjuvanticity analysis of CpG-LNP. LNP were formulated with DSPC, and DSG-PEG at an N/P of 10. (A) Experimental outline. (B1) ELISA dilution curves and (B2) corresponding AUC titers

of OVA protein-specific IgG, IgG1 and IgG2c antibody titers (n=5, mean ± SD). The dashed lines in the dilution curves of PBS group indicate the limit of detection of the assay. (C) Flow cytometry analysis of tetramer OVA-specific CD8+ T cells in the spleen one-week post boost immunization (n=5, mean ± SD). (D) Cytokines levels in serum samples determined by Bioplex cytokine assay (n=5, mean ± SD). Statistical analysis by one-way ANOVA; ****:p<0.0001, ***:p<0.001,**:p<0.01;*:p<0.05. Fold increase between CpG-LNP and soluble CpG are annotated.

CONCLUSION

In summary, CpG could successfully be encapsulated in LNP by electrostatic charge interaction with an ionizable cationic lipid. LNP formulation maintained the TLR9 agnostic activity of CpG in vitro. Intramuscular or subcutaneous injection of induced more robust innate immune activation in draining lymph nodes, compared to soluble CpG. Concomitantly, LNP(CpG) induced less innate activation in distal tissues, including the liver, which is the cause of dose-limiting toxicity of unformulated soluble CpG. In an immunization setting by admixing CpG-LNP with a model protein antigen, CpG-LNP showed to be a potent vaccine adjuvant being able to increase antigen-specific humoral and cellular immunity, with a strong isotype switching towards IgG2 isotype antibody production. Our findings provide a rational basis for using LNP-formulation for the delivery of CpG as a vaccine adjuvant to secondary lymphoid tissues.

In our current and future endeavors, we are focused on evaluating LNP(CpG) as an adjuvant for cancer and anti-hapten vaccines. Specifically, we are co-formulating the antigen and hapten to assess the effectiveness of LNP(CpG) as an adjuvant for each. Additionally, we are exploring the potential synergistic effect of co-formulating multiple TLR agonists in LNP to enhance the induction of innate and adaptive immunity.

EXPERIMENTAL SECTION

Materials

The ionizable lipid S-Ac7-DOG was synthesized as recently reported.[15] ODN1826 (CpG oligonucleotide) and FITC-labeled ODN1826 and Ovalbumin (OVA) were purchased from Invivogen (San Diego, United States). Cholesterol was purchased from Sigma-Aldrich (Saint Louis, USA). 1,2-distearoyl-sn-glycero-3-phosphocholine (18:0 PC, DSPC), dioleoylphosphatidylethanolamine (DOPE), 1,2-dimyristoyl-rac-glycero-3-methoxypolyethylene glycol-2000 (DMG-PEG 2000) and distearoyl-rac-glycerol-PEG2K (DSG-PEG 2000) were purchased from Avanti (Alabaster, USA).

Cells

Murine RAW-Blue cells were obtained from Invivogen (San Diego, USA). DC2.4 cells, an immortalized mouse dendritic cell line, were a kind gift from Dr. Ken Rock (Department of Pathology, University of Massachusetts Medical School).[24]

Mice

Female 6-8-week-old BALB/c mice and C57BL/6 mice were purchased from Janvier (France). Heterozygous IFN-β luciferase reporter (IFN-β+/Δβ-luc) mice with a BALB/c background were acquired from the Institute for Laboratory Animal Science at Hannover Medical School (Germany), the breeding was further maintained in house. All mice were housed in individually ventilated cages and had free access to feed and water. Mice were under isoflurane anesthesia (5% for induction and 2% for maintenance) during injections and bioluminescence imaging. Mice experiments were approved by the Ethics Committee of the Faculty of Veterinary Medicine, Ghent University (No. EC2022/053).

Formulation of CpG-LNPs

CpG-LNPs were fabricated by rapid mixing under vigorous stirring of an aqueous solution of CpG ODNs in 5 mM acetate buffer at pH 4.0 with an ethanolic solution containing ionizable lipid S-Ac-7-Dog, cholesterol, DSPC or DOPE, and DMG-PEG 2000 or DSG-PEG 2000 at a molar ratio of 50:38.5:10:1.5. CpG-LNP formulations were prepared at an N/P (N: mole of ionizable cationic nitrogen atoms in the ionizable lipid; P: mole of anionic phosphates in CpG) of 5:1 and 10:1, respectively. After mixing, LNPs were subjected to dialysis in a dialysis cassette (Thermo Scientific, Rockford, U.S.A) against PBS to remove ethanol. LNPs were concentrated using Amicon Ultra centrifugal filters (100 kD MWCO, Merck Millipore Ltd., Belgium). The CpG LNP formulations were then adjusted to 1 mg/mL of CpG and stored until further use.

CpG-LNP characterization

CpG LNP formulations were diluted 20-fold in HEPES buffer (5 mM, pH 7.4) and transferred into polystyrene cuvettes to measure particle size, polydispersity and zeta potential by dynamic light scattering (Zetasizer Nano-ZS, Malvern Panalytical Ltd., UK). The diameters are reported as Z-average values. The CpG ODNs encapsulation efficiency was measured by Quanti-it OliGreen assay (Life Technologies) according to the provided instruction manual. Fluorescence emission intensity was recorded on a PerkinElmer Multimode Plate Reader (PerkinElmer, Waltham, MA) set at 485 nm excitation and 525 nm emission. CpG encapsulation in LNP samples was calculated by comparing the fluorescence intensity of the

ssDNA-binding fluorescent dye OliGreen® in the absence (signal from unencapsulated CpG) and presence (signal from both encapsulated and unencapsulated) of 2% Triton X-100 (Merck, Germany) to dissolve the LNP. The encapsulation efficiency is calculated using the following equation: encapsulation efficiency (%) = ((Fluorescence) total – (Fluorescence) unencapsulated) / (Fluorescence) total × 100%. Recovery rate equation (%): actual amount of CpG by OliGreen/ Theoretical amount of CpG × 100%

Cryogenic Transmission Electron Microscopy (Cryo-TEM)

A 3 µL drop of the sample containing 1 mg/ml of CpG-LNPs was placed on a Quantifoil® R2/1 holey carbon film supported by a TEM copper grid (300 mesh, Quantifoil Micro Tools GmbH, Grossbloebichau, Germany) that was previously subjected to glow discharge treatment for 1 min at 6 mA (ELMO© Glow Discharge System, Agar Scientific Ltd, Essex, UK) to ensure better settling of the sample onto the grid. Excess liquid on the grid was removed by blotting with Whatman™ 1 filter paper (Whatman plc, Maidstone, UK) for 1 s, and the sample was rapidly plunged into liquid ethane at −176 °C using Cryoplunge™ 3 with GentleBlot™ system (Gatan Inc., Pleasanton, CA, USA) at 100% relative humidity. The vitrified samples were transferred with a Gatan 626 cryoholder (Gatan Inc., Pleasanton, CA, USA) and analyzed with a JEOL 1400+ transmission electron microscope (Jeol Ltd., Tokyo, Japan) equipped with LaB6 filament and TVIPS F416 charge-coupled device camera at 140 kV under low-dose conditions (∼10 e Å−2 s−1) at ×60000 magnification.

RAW-Blue innate immune activation assay

RAW-Blue cells were cultured in DMEM medium, supplemented with 10 % heat-inactivated fetal bovine serum (FBS), antibiotics (50 units/ml penicillin and 50 µg/ml streptomycin), 2 mM L-glutamine, 1 mM sodium pyruvate and 0.1 % Zeocin. Cells were incubated at 37 °C in a controlled and sterile environment of 95 % relative humidity and 5 % CO2. The cells were seeded in flat-bottom 96 well plates at a density of 90 000 cells per well (suspended in 180 µL). Next, cells 20 µL of LNP sample was added to the cells. This was done repeated in three-fold. After 24 h incubation at 37 °C, the NF-κB- and AP-1-inducible secreted embryonic alkaline phosphatase (SEAP) was assayed by collecting 50 µL of the induced cell supernatant followed by addition of 150 µL Quanti-Blue reagent solution according to the manufacturer's instructions. Finally, after 30 min incubation at 37 °C, the secreted embryonic alkaline phosphatase levels were determined by UV-Vis spectrophotometry using a microplate reader at 620 nm.

MTT cell viability assay

DC2.4 cells were cultured in RPMI-glutamax, supplemented with 10 % FBS, 1 % penicillin/streptomycin and 1 mM sodium pyruvate. DC2.4 cells were seeded in 96 well plates

at a density of 10 000 cells per well (suspended in 180 µL culture medium) and allowed to adhere overnight. Subsequently, cells were treated for 24 hours with 20 µL of different concentrations of LNP sample as described above. PBS and DMSO were receptively used as negative control (100 % viability) and positive control (0 % viability). After incubation at 37 °C, the medium was removed, and the cells were washed with 200 µL PBS. To each well 100 µL of diluted MTT solution was added and incubated for 2 h at 37 °C. Next, the diluted MTT solution was aspirated, and the formed formazan crystals were dissolved by addition of 50 µL DMSO. Quantification was done by measuring the absorbance at 590 nm using a microplate reader. The MTT stock solution was prepared by dissolving 50 mg MTT in 10 mL PBS. After filtration (membrane 0.22 µm), a 1/5 dilution in culture medium was done and the diluted MTT solution was used in this assay.

Flow cytometry of in vitro cell uptake

DC2.4 cells were seeded in 96 well plates at a density of 10 000 cells per well (suspended in 180 µL culture medium) and allowed to adhere overnight. Subsequently, cells were treated for 24 hours with 20 µL of different concentrations of FITC-labelled CpG-LNP as described above. The next day, the plate was centrifuged for 5 min at 300 g. The supernatant was removed from the wells by flipping the plate over onto absorbent paper. Thereafter, 30 µL TrypLE Select (Gibco, Grand Island, USA) was added to the wells. After 5 min incubation, 200 µL eBioscience Flow Cytometry Staining Buffer (Invitrogen, Massachusetts, USA) was added. The content of each well was pipetted a few times up and down to obtain a single cell dispersion before collecting the cells for flow cytometry analysis. The analysis was performed using an Accuri C6 Flow cytometer (BD Biosciences, Franklin Lakes, USA). The cell population was analyzed based on FITC excitation/emission using a blue laser with a wavelength of 488 nm. Data processing was performed using the FlowJo software package.

Confocal microscopy

DC2.4 cells were seeded in WillCo-Dish glass bottom dishes (WillCo Wells BV, Amsterdam, The Netherlands) at a density of 2 × 104 cells in 180 µL and allowed to adhere overnight. Cells were then treated with 20 µL of FITC-labeled soluble CpG or CpG-LNPs at a final CpG concentration of 1 µg/mL and continued to culture overnight in a CO2 incubator. After that, the cell medium was aspirated and cells were washed with DPBS followed by addition of 150 µL 4% paraformaldehyde (PFA). After 15 min incubation, the PFA was aspirated and the wells were washed with DPBS. Next, cells were stained during 45 min by adding 150 µL DPBS containing 1.5 µL Hoechst (Invitrogen, Massachusetts, USA). The staining solution was aspirated and the dishes were washed with DPBS. Finally, 150 µL DPBS was left on the dishes to prevent the cells from dehydrating. Cells were imaged using a Leica DMI6000B microscope

connected to an Andor DSD2 confocal scanner. A 63 x (1.40 NA) oil-immersion objective was used to record Z-stacks. Image processing was performed using ImageJ the software package and the Microvolution deconvolution algorithm.

Bioluminescence imaging of the in vivo CpG-triggered IFN-β response

Heterozygous IFNβ+/Δβ-luc luciferase reporter mice with a BALB/c background, aged 7-9 weeks, were used. Unformulated soluble CpG, DMG-PEG or DSG-PEG containing CpG-LNPs or blank LNP (i.e. LNP without CpG) was injected subcutaneously in the footpad (dose of 2 µg CpG in 20 µL PBS) or intramuscularly in the gastrocnemius muscle (dose of 10 µg of CpG in 100 µL PBS). CpG concentrations were equalized in all samples at 100 µg CpG/mL. For in vivo bioluminescence imaging at 4, 24 and 48 hours post subcutaneous injection, or 4 and 24h post intramuscular injection of CpG formulations, mice were injected subcutaneously with 200 µL D-luciferin (Perkin Elmer, Waltham, USA) and in vivo luminescence imaging was recorded 12 min later using an IVIS Lumina II imaging system. The luminescence in the draining popliteal lymph node (for the case of subcutaneous injection) or injection site (for the case of intramuscular injection) and the full-body luminescence were quantified using the LivingImage 4.4 software package.

Analysis of in vivo lymphatic translocation and innate activation

To address lymphatic drainage after subcutaneous or intramuscular injection, 20 µL or 100 µL of FITC-labelled soluble CpG, FITC-labelled CpG LNP, and blank LNP were injected into the footpad or gastrocnemius muscle, respectively, of female IFNβ+/Δβ-luc mice. At 24 h after injections, mice were sacrificed, and popliteal lymph nodes (subcutaneous injection in footpad injection) and iliac lymph nodes (intramuscular injection in gastrocnemius muscle) were isolated for flow cytometry. A single cell suspension was prepared form the dissected popliteal lymph nodes for analysis by flow cytometry. Isolated lymph nodes were collected in ice cold PBS, smashed through 70 µm cell strainers (VWR International, 732-2758), washed with PBS and stained for 30 min at 4°C with following primary labeled antibodies: CD86, CD40. After identification of singlets, DCs were identified by activation markers CD40 (APC-CD40) and CD86 (PacificBlue-CD86). Live dead ratios were determined by staining with fixable dead/live staining and 123count ebeads were added to determine relative cell numbers. Samples were finally analyzed on a flow cytometer (BD LSR Fortessa). Data were processed using the FlowJo software package.

In vivo adjuvanticity assessment

Pre-shaved female C57BL6 mice (7-8 weeks) were anesthetized by inhalation of isoflurane and immunized by intramuscular injection in the quadriceps of 50 µg OVA protein with the indicated adjuvant formulations in a final volume of 100 µL in PBS. The control mice cohort

received equal volume of PBS. The immunization schedule is depicted in Figure 6a. Booster immunizations were given in mice at 3 and 6 weeks post prime immunization, and mice were bled at 3 and 6 weeks after the first immunization. At week 7, mice were sacrificed and their spleens were harvested to assess T cell response by OVA tetramer staining analysis.

OVA specific antibody titers

OVA-specific antibody titers were determined by ELISA assay with a commercially available ELISA buffer kit (Invitrogen). In more details, uncoated 96-well ELISA plates (Biolegend) were coated by addition of 50 ng of OVA to each well, followed by overnight incubation at 4 °C and subsequently blocking with assay buffer for 1 h at room temperature. Five-fold serial dilutions of the serum samples were made (starting from a 100-fold dilution) and 100 µL of these dilutions was added per well. After 1 h of incubation at room temperature, the plates were washed four times with wash solution. Next, 100 µl of goat anti-mouse IgG horseradish peroxidase (HRP)-conjugated secondary antibody (Tebu-bio) or goat anti-mouse IgG1 HRP-conjugated secondary antibody (Invitrogen) in 1:3000 dilution was added to the wells and incubated for 1 h at room temperature. To determine the OVA-specific IgG2c titers, goat anti-mouse IgG2c (Invitrogen, Fisher Scientific) in 1:3000 dilution was added to the plates followed by three times with wash solution, and HRP-conjugated rabbit anti-goat IgG (H+L) ((abcam) in 1:3000 dilution was applied to the plates. Subsequently, the wells were washed five times and then incubated with 100 µL of 3,3',5,5'-Tetramethylbenzidine (TMB) substrate at room temperature. The enzymatic conversion of TMB was stopped after 15 min by adding 100 µL of stop solution containing 0.16 M sulfuric acid, and the absorbance was measured at 450 nm using an EnSight microplate reader (PerkinElmer, United States). The antibody titers were defined as the area under the curve (AUC) of the ELISA dilution curves.

OVA-specific cellular immune response

Splenocytes were isolated seven weeks after the prime immunization and 106 cells were treated with anti-CD3 antibody (eBiosciences, 11-0033-82), anti-CD8 antibody (eBiosciences, 25-0081-82) and PE-conjugated OVA H-2 Kb tetramer epitope (SIINFEKL) (Immudex). Live dead ratios were determined by staining with fixable dead/live staining and 123count ebeads were added to determine relative cell numbers. Cells were analyzed on a flow cytometer (BD Lsrfortessa). Data were processed using the FlowJo software package.

Bio-Plex cytokine assay

Serum samples were collected at 6 hours after the final immunization. Cytokines (IL-1b, IL-4, IL-6, IL-10, IL-12(p70), IFN-γ, MCP-1 and TNF-α) were measured on a Luminex Bioplex suspension array system (Bio-Rad) according to the manufacturer's instructions. Briefly, 1/3 diluted serum samples were added to magnetic capture beads (Biorad) and incubated for 2 h

at room temperature. After incubation, the beads were washed, and detection antibodies (Biorad) were added to the wells. After 1 h incubation the beads were washed again and incubated for 30 min with streptavidin-PE (Biorad). Finally, the samples were measured on a Bio-Plex 200 Systems (Bio-Rad). Cytokine concentrations were analyzed using standard curves and expressed in pg/mL.

Statistical analysis

Statistical analyses were performed with GraphPad Prism software (version 8.3, GraphPad Software Inc., CA, USA). The longitudinal experiments of different animal groups were analyzed using repeated-measures two-way ANOVA, corrected for multiple comparisons (Bonferroni method). Differences between two groups were compared with student's t test (non-parametric Mann-Whitney U test). Data in the study are represented as means ± SEM, unless otherwise mentioned. A p-value of below 0.05 is considered statistically significant difference (*p<0.05, **p<0.01, ***p<0.001, ****p<0.0001).

ACKNOWLEDGEMENTS

ZZ is supported by a postdoctoral grant from the Research Foundation—Flanders (FWO-Vlaanderen, 12K0323N). B.G.D.G. acknowledges funding from the European Research Council (ERC) under the European Union's Horizon 2020 research and innovation program (grant N 817938).

REFERENCES

[1] aD. J. Irvine, M. C. Hanson, K. Rakhra, T. Tokatlian, Chem Rev 2015, 115, 11109-11146; bJ. J. Moon, H. Suh, A. Bershteyn, M. T. Stephan, H. Liu, B. Huang, M. Sohail, S. Luo, S. H. Um, H. Khant, J. T. Goodwin, J. Ramos, W. Chiu, D. J. Irvine, Nat Mater 2011, 10, 243-251; cR. Kuai, L. J. Ochyl, K. S. Bahjat, A. Schwendeman, J. J. Moon, Nat Mater 2017, 16, 489-496; dA. de Titta, M. Ballester, Z. Julier, C. Nembrini, L. Jeanbart, A. J. van der Vlies, M. A. Swartz, J. A. Hubbell, Proc Natl Acad Sci U S A 2013, 110, 19902-19907; eQ. Zeng, J. M. Gammon, L. H. Tostanoski, Y. C. Chiu, C. M. Jewell, ACS Biomater Sci Eng 2017, 3, 195-205; fS. Barman, F. Borriello, B. Brook, C. Pietrasanta, M. De Leon, C. Sweitzer, M. Menon, S. D. van Haren, D. Soni, Y. Saito, E. Nanishi, S. Yi, S. Bobbala, O. Levy, E. A. Scott, D. J. Dowling, ACS Chem Biol 2022, 17, 2559-2571.

[2] aG. P. Amarante-Mendes, S. Adjemian, L. M. Branco, L. C. Zanetti, R. Weinlich, K. R. Bortoluci, Front Immunol 2018, 9, 2379; bR. Medzhitov, Nature 2007, 449, 819-826.

[3] aB. A. Beutler, Blood 2009, 113, 1399-1407; bC. A. Thaiss, M. Levy, S. Itav, E. Elinav, Trends Immunol 2016, 37, 84-101.

[4] aJ. Jie, Y. Zhang, H. Zhou, X. Zhai, N. Zhang, H. Yuan, W. Ni, G. Tai, Int J Mol Sci 2018, 19; bA. M. Krieg, Annu Rev Immunol 2002, 20, 709-760; cT. Sacher, P. Knolle, T. Nichterlein, B. Arnold, G. J. Hammerling, A. Limmer, Eur J Immunol 2002, 32, 3628-3637.

[5] aN. Hanagata, Int J Nanomedicine 2012, 7, 2181-2195; bJ. Vollmer, A. M. Krieg, Adv Drug Deliv Rev 2009, 61, 195-204.

[6] aR. S. Chu, O. S. Targoni, A. M. Krieg, P. V. Lehmann, C. V. Harding, J Exp Med 1997, 186, 1623-1631; bD. M. Klinman, Nat Rev Immunol 2004, 4, 249-258.

[7] aC. Bode, G. Zhao, F. Steinhagen, T. Kinjo, D. M. Klinman, Expert Rev Vaccines 2011, 10, 499-511; bY. M. Murad, T. M. Clay, BioDrugs 2009, 23, 361-375.

[8] aC. Manegold, N. van Zandwijk, A. Szczesna, P. Zatloukal, J. S. K. Au, M. Blasinska-Morawiec, P. Serwatowski, M. Krzakowski, J. Jassem, E. H. Tan, R. J. Benner, A. Ingrosso, S. J. Meech, D. Readett, N. Thatcher, Ann Oncol 2012, 23, 72-77; bV. Hirsh, L. Paz-Ares, M. Boyer, R. Rosell, G. Middleton, W. E. Eberhardt, A. Szczesna, P. Reiterer, M. Saleh, O. Arrieta, E. Bajetta, R. T. Webb, J. Raats, R. J. Benner, C. Fowst, S. J. Meech, D. Readett, J. H. Schiller, J Clin Oncol 2011, 29, 2667-2674.

[9] G. H. Lee, S. G. Lim, Expert Rev Vaccines 2021, 20, 487-495.

[10] S. Shirai, M. Shibuya, A. Kawai, S. Tamiya, L. Munakata, D. Omata, R. Suzuki, T. Aoshi, Y. Yoshioka, Front Immunol 2019, 10, 3018.

[11] J. Meng, P. Zhang, Q. Chen, Z. Wang, Y. Gu, J. Ma, W. Li, C. Yang, Y. Qiao, Y. Hou, L. Jing, Y. Wang, Z. Gu, L. Zhu, H. Xu, X. Lu, M. Gao, Adv Mater 2022, 34, e2202168.

[12] M. H. Lahoud, F. Ahmet, J. G. Zhang, S. Meuter, A. N. Policheni, S. Kitsoulis, C. N. Lee, M. O'Keeffe, L. C. Sullivan, A. G. Brooks, R. Berry, J. Rossjohn, J. D. Mintern, J. Vega-Ramos, J. A. Villadangos, N. A. Nicola, M. C. Nussenzweig, K. J. Stacey, K. Shortman, W. R. Heath, I. Caminschi, Proc Natl Acad Sci U S A 2012, 109, 16270-16275.

[13] aJ. P. Bost, H. Barriga, M. N. Holme, A. Gallud, M. Maugeri, D. Gupta, T. Lehto, H. Valadi, E. K. Esbjorner, M. M. Stevens, S. El-Andaloussi, ACS Nano 2021, 15, 13993-14021; bP. R. Cullis, M. J. Hope, Mol Ther 2017, 25, 1467-1475; cL. Schoenmaker, D. Witzigmann, J. A. Kulkarni, R. Verbeke, G. Kersten, W. Jiskoot, D. J. A. Crommelin, Int J Pharm 2021, 601, 120586.

[14] M. G. Alameh, I. Tombacz, E. Bettini, K. Lederer, C. Sittplangkoon, J. R. Wilmore, B. T. Gaudette, O. Y. Soliman, M. Pine, P. Hicks, T. B. Manzoni, J. J. Knox, J. L. Johnson, D. Laczko,

H. Muramatsu, B. Davis, W. Meng, A. M. Rosenfeld, S. Strohmeier, P. J. C. Lin, B. L. Mui, Y. K. Tam, K. Kariko, A. Jacquet, F. Krammer, P. Bates, M. P. Cancro, D. Weissman, E. T. Luning Prak, D. Allman, M. Locci, N. Pardi, Immunity 2021, 54, 2877-2892 e2877.

[15] Y. C. Emily De Lombaerde, Tingting Ye, Zifu Zhong, Alexander Lamoot, Stefaan De Koker, Bruno De Geest, manuscript in preparation.

[16] X. Zhu, W. Tao, D. Liu, J. Wu, Z. Guo, X. Ji, Z. Bharwani, L. Zhao, X. Zhao, O. C. Farokhzad, J. Shi, Theranostics 2017, 7, 1990-2002.

[17] K. J. Hassett, J. Higgins, A. Woods, B. Levy, Y. Xia, C. J. Hsiao, E. Acosta, O. Almarsson, M. J. Moore, L. A. Brito, J Control Release 2021, 335, 237-246.

[18] M. H. Y. Cheng, J. Leung, Y. Zhang, C. Strong, G. Basha, A. Momeni, Y. Chen, E. Jan, A. Abdolahzadeh, X. Wang, J. A. Kulkarni, D. Witzigmann, P. R. Cullis, Adv Mater 2023, e2303370.

[19] G. T. Szabo, A. J. Mahiny, I. Vlatkovic, Mol Ther 2022, 30, 1850-1868.

[20] B. L. Mui, Y. K. Tam, M. Jayaraman, S. M. Ansell, X. Du, Y. Y. Tam, P. J. Lin, S. Chen, J. K. Narayanannair, K. G. Rajeev, M. Manoharan, A. Akinc, M. A. Maier, P. Cullis, T. D. Madden, M. J. Hope, Mol Ther Nucleic Acids 2013, 2, e139.

[21] D. L. Thibault, K. L. Graham, L. Y. Lee, I. Balboni, P. J. Hertzog, P. J. Utz, Arthritis Res Ther 2009, 11, R112.

[22] H. Liu, K. D. Moynihan, Y. Zheng, G. L. Szeto, A. V. Li, B. Huang, D. S. Van Egeren, C. Park, D. J. Irvine, Nature 2014, 507, 519-522.

[23] B. Song, S. Aoki, C. Liu, T. Susukida, K. Ito, Toxicol Sci 2018, 162, 713-723.

[24] Z. Shen, G. Reznikoff, G. Dranoff, K. L. Rock, J Immunol 1997, 158, 2723-2730.

SUPPORTING INFORMATION

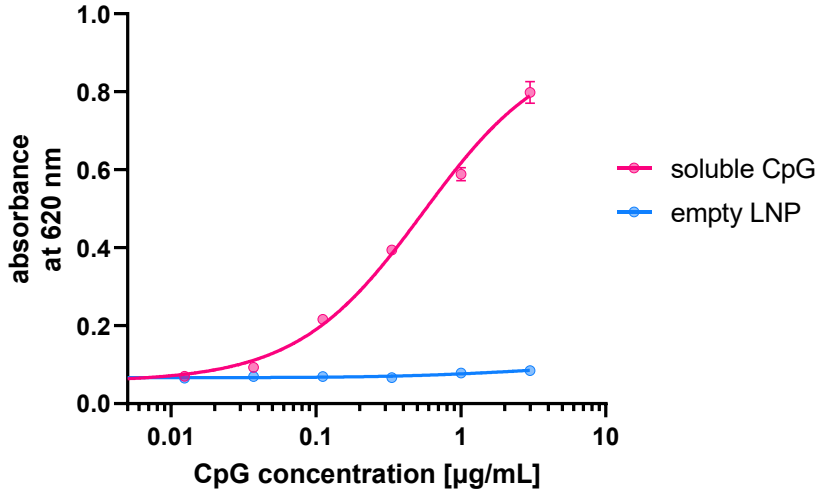

Figure S1. TLR agonistic activity of empty LNP formulations measured by the RAW-Blue NF-kB reporter cell assay.

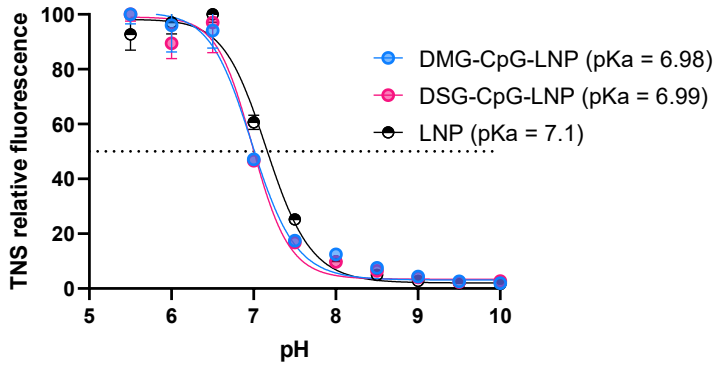

Figure S2. pKa (determined as IC50 values) of CpG LNP formulation determined by TNS assay.

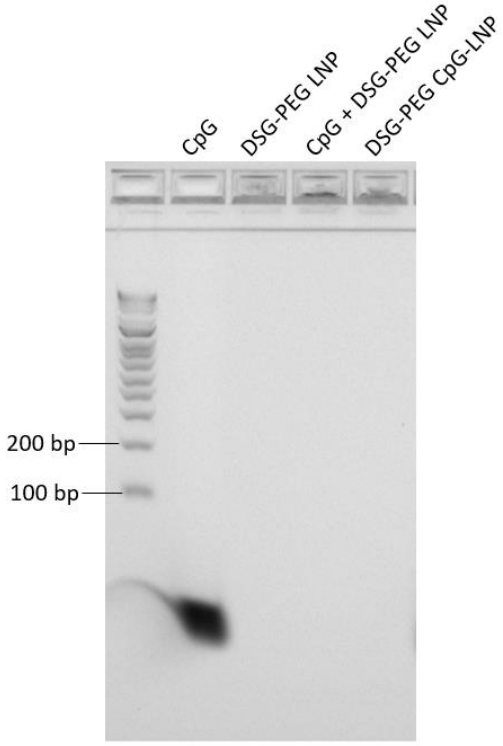

Figure S3. Agarose gel electrophoresis of soluble CpG, empty LNP (DSG-PEG LNP), CpG admixed with DSG-PEG LNP and DSG-PEG CpG-LNP. Notably, 4th lane shows that soluble CpG can be bound by admixing with empty LNP.

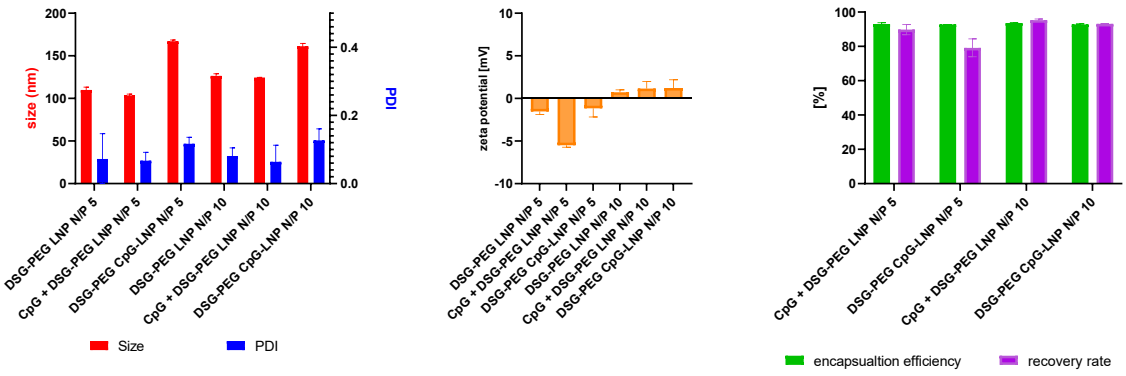

Figure S4. characterization of CpG-LNP and CpG admixed with empty LNP. (A) DLS analysis of Z-average diameter and PDI, (B) zeta-potential and (C) encapsulation efficiency and recovery of LNP formulations measured by OliGreen assay (n=3, mean ± SD). (LNPs: DSPC/DSG-PEG/10:1 or DSPC/DSG-PEG/5:1).

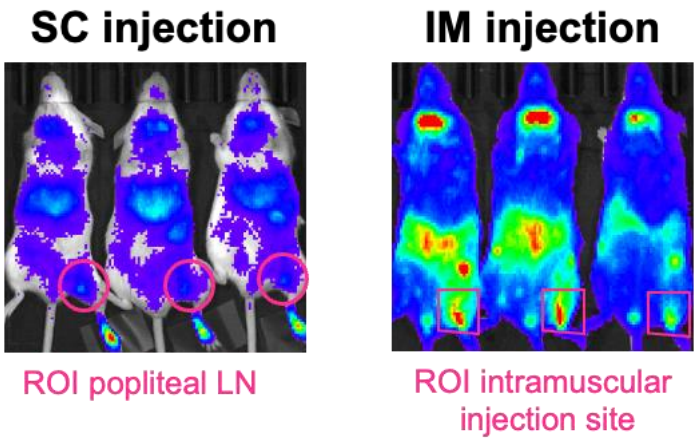

Figure S4. Annotation of the region of interests (ROIs) of SC or IM, respectively, injected mice.

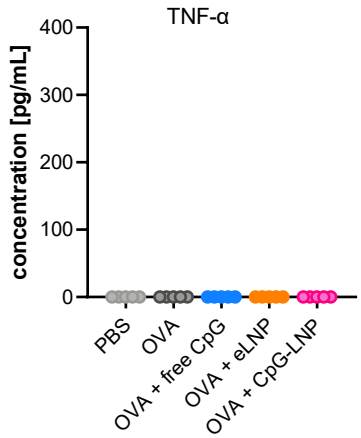

Figure S5. TNF-α levels in mouse serum determined by Bioplex cytokine assay (n=5, mean ± SD).

Table S1. Statistical analysis of Figure 2 by one-way ANOVA. ****:p<0,0001; ***:p<0,001; **:p<0,01; *:p<0,05).

size	significance	P Value
LNP 7 vs. LNP 1	ns	0.9989
LNP 7 vs. LNP 2	****	<0.0001
LNP 7 vs. LNP 3	***	0.0008
LNP 7 vs. LNP 4	****	<0.0001
LNP 7 vs. LNP 5	***	0.0002
LNP 7 vs. LNP 6	***	0.0003
LNP 7 vs. LNP 8	***	0.0002
LNP 7 vs. LNP 9	ns	0.1216

PDI	significance	P Value
LNP 7 vs. LNP 1	ns	>0.9999
LNP 7 vs. LNP 2	ns	>0.9999
LNP 7 vs. LNP 3	ns	>0.9999
LNP 7 vs. LNP 4	ns	>0.9999
LNP 7 vs. LNP 5	ns	>0.9999
LNP 7 vs. LNP 6	ns	>0.9999
LNP 7 vs. LNP 8	ns	>0.9999
LNP 7 vs. LNP 9	ns	>0.9999

encapsulation efficiency	significance	P Value
LNP 7 vs. LNP 1	***	0.0009
LNP 7 vs. LNP 2	*	0.0134
LNP 7 vs. LNP 3	ns	0.96
LNP 7 vs. LNP 4	*	0.0325
LNP 7 vs. LNP 5	ns	0.4668
LNP 7 vs. LNP 6	ns	0.1182
LNP 7 vs. LNP 8	ns	0.0877

recovery rate	significance	P Value
LNP 7 vs. LNP 1	****	<0.0001
LNP 7 vs. LNP 2	****	<0.0001
LNP 7 vs. LNP 3	****	<0.0001
LNP 7 vs. LNP 4	*	0.0219
LNP 7 vs. LNP 5	****	<0.0001
LNP 7 vs. LNP 6	ns	0.1629
LNP 7 vs. LNP 8	*	0.0121

Table S2. Statistical analysis of Figure 3B by one-way ANOVA. ****:p<0,0001; ***:p<0,001; **:p<0,01; *:p<0,05).

EC50	significance	P Value
LNP7 vs. naked CpG	**	0.0015
LNP7 vs. LNP1	****	<0.0001
LNP7 vs. LNP2	****	<0.0001
LNP7 vs. LNP3	*	0.0263
LNP7 vs. LNP4	*	0.0146
LNP7 vs. LNP5	****	<0.0001
LNP7 vs. LNP6	****	<0.0001
LNP7 vs. LNP8	ns	0.9905

Table S3. Statistical analysis of Figure 4A by two-way ANOVA. ****:p<0,0001; ***:p<0,001; **:p<0,01; *:p<0,05).

50 ng CpG

2 h	Summary	P Value
CpG vs. DMG-PEG LNP(CpG)	**	0.0032
CpG vs. DSG-PEG LNP(CpG)	***	0.0009
DMG-PEG LNP(CpG) vs. DSG-PEG LNP(CpG)	ns	0.2406
6 h		
CpG vs. DMG-PEG LNP(CpG)	ns	0.8594
CpG vs. DSG-PEG LNP(CpG)	*	0.0457
DMG-PEG LNP(CpG) vs. DSG-PEG LNP(CpG)	ns	0.5663
20 h		
CpG vs. DMG-PEG LNP(CpG)	ns	0.1246
CpG vs. DSG-PEG LNP(CpG)	ns	0.3798
DMG-PEG LNP(CpG) vs. DSG-PEG LNP(CpG)	ns	0.2003
24 h		
CpG vs. DMG-PEG LNP(CpG)	****	<0.0001

CpG vs. DSG-PEG LNP(CpG)	**	0.0093
DMG-PEG LNP(CpG) vs. DSG-PEG LNP(CpG)	****	<0.0001

200 ng CpG

2 h	Summary	P Value
CpG vs. DMG-PEG LNP(CpG)	***	0.0005
CpG vs. DSG-PEG LNP(CpG)	ns	0.2432
DMG-PEG LNP(CpG) vs. DSG-PEG LNP(CpG)	***	0.0002
6 h		
CpG vs. DMG-PEG LNP(CpG)	ns	0.8456
CpG vs. DSG-PEG LNP(CpG)	***	0.0006
DMG-PEG LNP(CpG) vs. DSG-PEG LNP(CpG)	**	0.0069
20 h		
CpG vs. DMG-PEG LNP(CpG)	ns	0.1092
CpG vs. DSG-PEG LNP(CpG)	*	0.0104
DMG-PEG LNP(CpG) vs. DSG-PEG LNP(CpG)	***	0.001
24 h		

CpG vs. DMG-PEG LNP(CpG)	***	0.0007
CpG vs. DSG-PEG LNP(CpG)	****	<0.0001
DMG-PEG LNP(CpG) vs. DSG-PEG LNP(CpG)	****	<0.0001